NJC

RSC Publishing

PAPER

π-Interactions as a tool for an easy deposition of *meso*-tetraferrocenylporphyrin on surfaces†‡

Cite this: *New J. Chem.*, 2013, **37**, 3535

Andrea Vecchi,*[a] Valentina Grippo,[a] Barbara Floris,[a] Andrea Giacomo Marrani,[b] Valeria Conte[a] and Pierluca Galloni*[a]

Received (in Montpellier, France) 15th May 2013,
Accepted 24th July 2013

DOI: 10.1039/c3nj00519d

www.rsc.org/njc

A bottom-up approach was employed to prepare novel Self-Assembled Monolayers (SAMs) in which a naphthyl moiety acted as a ''π-binder'' for unfunctionalised *meso*-tetraferrocenylporphyrin (H_2TFcP). Four naphthalene derivatives with an appropriate functional group were synthesized and SAMs were prepared both on gold and ITO surfaces. Mixed H_2TFcP–naphthalene films were thoroughly characterized using UV-Vis, XPS and electrochemical techniques. In particular, angle-dependent XPS experiments revealed an almost perpendicular orientation of the porphyrin on surfaces, suggesting that an intercalation occurred among naphthalene units. A large amount of porphyrin was deposited on both the surfaces (in the order of 10^{-10} mol × cm^{-2}), comparable to that afforded by more conventional covalent linkages. However, significant differences in homogeneity between SAMs on gold and ITO resulted in a diverse electrochemical behaviour. The electrochemical activity of the oxidised porphyrin was restored by prolonged exposure of the modified gold electrode (tens of seconds) to a negative potential, whereas no response was detected after the same treatment on ITO. This novel approach provides a general and versatile strategy to bind *meso*-substituted porphyrins on a pre-formed monolayer without the necessity for further functionalisations.

Introduction

Aromatic–aromatic or π-interactions are fundamental non-covalent forces, which are ubiquitous in Nature and play a significant role in stabilisation of macromolecules and in their biological activity. As a remarkable example π–π stacking of the bases is considered to be the major free energy contribution in stabilising the double helix arrangement of DNA.[1] The interactions between aromatic residues are essential for structural stabilisation of proteins, protein–protein recognition, ligand binding and folding.[2] It was estimated that about 60% of aromatic residues are involved in π-interactions, 80% of which participate in a network of at least three interacting side chains. An average optimal distance between interacting rings was found to be 5 Å and the most recurring geometry is the edge-to-face (or T-shaped).[3] Furthermore, aromatic–aromatic interactions are known to be responsible for self-aggregation of chlorophyll dyes in photosynthetic organisms. For instance, cyclic dye arrays and rod-like aggregates of hundreds of dyes were found in purple[4] and green bacteria respectively.[5] These outstanding supramolecular architectures allow an efficient energy transfer between chromophores upon photo-excitation.[6] This latter feature has stimulated the idea that the extended π-conjugation of the tetrapyrrolic skeleton of porphyrins could be exploited as a building block to build advanced functional materials with peculiar optical and electronic properties. Since then, several examples of supramolecular π-complexes of porphyrins with carbon nanostructures were reported.[7] Among the examples, one of the most intriguing supramolecular systems regards a host–guest complex between a porphyrin nanobarrel and fullerene C_{60}. The nanobarrel is constituted by a cyclic porphyrin tetramer whose cavity (14 Å of diameter) was designed to encapsulate C_{60}.[8]

The aromatic–aromatic interaction between porphyrins and carbon-based nanomaterials has been elegantly exploited, in a series of papers[9] by Komatsu and co-workers, to separate Single Walled Carbon NanoTubes (SWCNTs) according to their handedness and diameter. The rational design of chiral diporphyrin ''clamps'' allowed the chiral resolution providing satisfactory enantiomeric excesses. Finally, highly efficient photocurrent generating systems were assembled on surfaces taking advantage of the aforementioned non-covalent interactions

[a] *Dipartimento di Scienze e Tecnologie Chimiche, Università di Roma ''Tor Vergata'', Via della Ricerca Scientifica snc, 00133 Rome, Italy. E-mail: galloni@scienze.uniroma2.it, andrea.vecchi@uniroma2.it; Fax: +39 0672594328*

[b] *Dipartimento di Chimica, Università degli Studi di Roma ''La Sapienza'', Piazzale Aldo Moro 5, 00185 Rome, Italy*

† Dedicated to Prof. Bernard Meunier on occasion of his retirement.

‡ Electronic supplementary information (ESI) available: Synthesis of naphthalene derivatives, UV-Vis spectra, CV, DPV and XPS data. See DOI: 10.1039/c3nj00519d

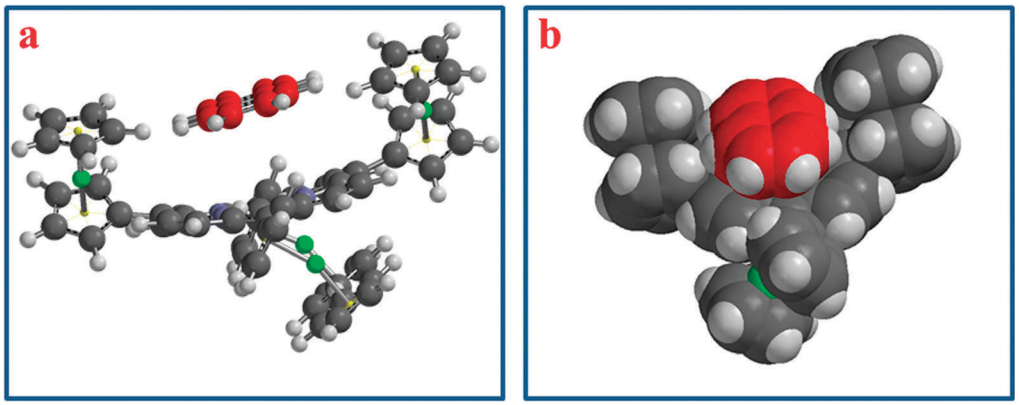

Fig. 1 Balls and sticks (a) and space filling (b) representation of the *meso*-tetraferrocenylporphyrin–naphthalene (red) π-complex according to PM3 calculations.

between porphyrins and fullerenes,[10] or between porphyrins and SWCNTs[11] or nanodiamonds.[12]

Among the huge variety of possible substituents that can be introduced at the periphery of the porphyrin *core*, metallocenyl units endow these compounds with unique photophysical and electrochemical properties and have drawn large attention in the last two decades.[13] The overwhelming majority of reported metallocenyl-substituted porphyrins are composed of redox-active ferrocenyl moieties appended to the *meso* or to the β positions of the tetrapyrrolic macrocycle. Besides the well-known potentialities brought about by these substituents (redox-driven fluorescence switches[14] or sensors,[15] photo-induced electron transfer processes[16] for solar energy conversion[17] and molecular-based multibit information storage devices[18]), additional exciting perspectives are expected if ferrocenyl groups are efficiently conjugated through the porphyrin *core*. Indeed, these compounds exhibit strong metal–metal coupling which is responsible for multiredox processes, magnetic coupling and unpaired electron density migration. The corresponding mixed-valence species are characterized by redox-dependent spectroscopic features and were indicated as candidates for fluorescence and optical switches in the NIR region of the spectrum.[19] Also, electronic communication between equivalent redox centres in *meso*-polyferrocenylporphyrins results in the progressive removal of individual electrons.[19–21] The accessibility of multiple cationic states is largely desirable in the field of molecular memories, since each redox state is regarded as single elemental data storage.

Our recent efforts were aimed at the preparation of novel *meso*-tetraferrocenylporphyrin-containing Self-Assembled Monolayers (SAMs).[22] Although fascinating results in terms of porphyrin density and electrochemical properties were obtained, their application in real world's nanoscale devices might be limited by low yield synthesis and laborious purification procedures of the porphyrin precursor. The synthetic limiting step prompted us to explore novel routes to deposit tetraferrocenylporphyrins (TFcPs) on gold and Indium Tin Oxide (ITO) surfaces starting from low cost and unfunctionalised materials. To this purpose, we decided to exploit aromatic–aromatic interactions to prepare mixed naphthalene–H_2TFcP-containing films. To the best of our knowledge, this is the first attempt to attach an unfunctionalised and metal-free porphyrin on surfaces just taking advantage of simple non-covalent interactions. The choice of naphthalene as "π-binder" is due to the perfect accommodation of its carbon skeleton within the "cradle" generated by two *trans* ferrocenyl groups of the saddle-shaped α,β,α,β-atropoisomer as predicted by semi-empirical PM3 geometry optimization (see Fig. 1). A preliminary examination of the association in solution revealed the formation of a π-complex between H_2TFcP and naphthalene. Such an association seems to facilitate the oxidation of the porphyrin by the atmospheric dioxygen. However, the solution behaviour of these species is somewhat ambiguous and its elucidation is currently under investigation in our laboratories.

Results and discussion

Four naphthalene derivatives (see Fig. 2) were appropriately designed for attaching on gold and ITO surfaces. The former was functionalised taking advantage of the easy *in situ* cleavage of the thioacetyl group, whereas a carboxylate was introduced to deposit naphthalene on ITO. Moreover, since α and β isomers are expected to assume a different geometry on surfaces, their affinity toward H_2TFcP might be extremely different. For this reason both isomers were used to decorate gold and ITO and their binding ability was evaluated. Functionalisation of

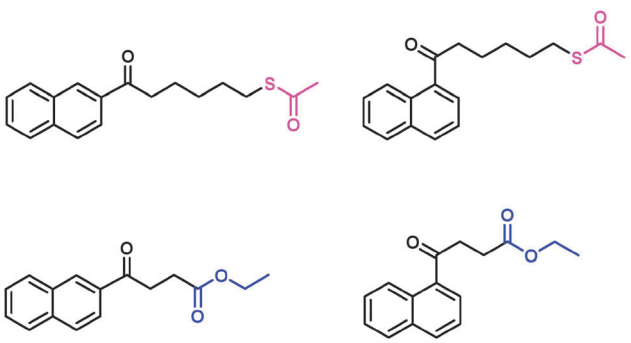

Fig. 2 Structures of the four naphthalene derivatives. 1- and 2- (6-acetylthiohexanoyl)naphthalene (first row) were used to functionalise gold, whereas ethyl 4-(1- and 2-naphthyl)-4-oxobutanoate (second row) were deposited on ITO.

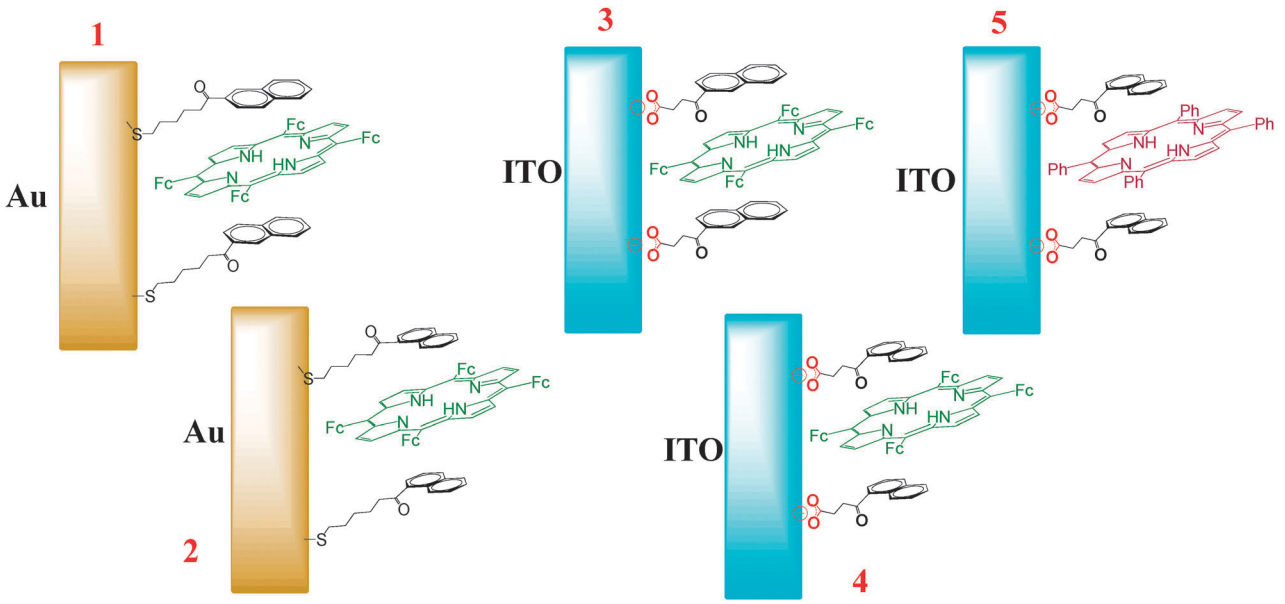

Fig. 3 Possible sandwich-like structures for SAMs prepared from: (1) 2-(6-acetylthiohexanoyl)–naphthalene and H_2TFcP; (2) 1-(6-acetylthio-hexanoyl)–naphthalene and H_2TFcP; (3) 4-(2-naphthyl)-4-oxobutanoate and H_2TFcP; (4) 4-(1-naphthyl)-4-oxobutanoate and H_2TFcP; (5) 4-(1-naphthyl)-4-oxobutanoate and *meso*-tetraphenylporphyrin.

naphthalene was carried out with the classical Friedel–Crafts conditions for acyl chlorides and anhydrides.[23] Although electrophilic substitutions of naphthalene are expected mainly at the α position, a substantial prevalence of the β isomer was obtained suggesting a thermodynamic control in these reactions. The chromatographic purification of the isomers was the most challenging step. The isolation of carboxy-substituted naphthalenes required the esterification of the acidic group in order to make separation of isomers feasible. H_2TFcP was synthesized according to a well-established procedure[24] under modified Lindsey's conditions.[25]

SAMs were prepared using a two-step procedure consisting of the formation of a naphthalene monolayer followed by its immersion in a porphyrin solution. As for ITO functionalization, an *in situ* basic hydrolysis was carried out to restore the required carboxylate group. The homogeneity of the naphthalene SAM after the first preparation step was qualitatively evaluated through the cyclic voltammetry of a solution of $K_3[Fe(CN)_6]$ using the modified gold foil as the working electrode. If the monolayer is densely packed, the electron transfer between the redox probe and the electrode is hampered and the expected peaks of ferricyanide are absent in the voltammogram.[26] This corresponds to the situation observed for the SAMs prepared from 1- and 2- (6-acetylthiohexanoyl)naphthalene and no difference in homogeneity was detected between α and β isomers (see Fig. S9 in ESI‡). Four different H_2TFcP-based sandwich-like films were prepared using α and β-naphthalene derivatives. In particular, a couple of isomers were assembled on gold, while the other couple were attached to ITO. Besides these, an extra *meso*-tetraphenylporphyrin-containing film was prepared on ITO using the ethyl 4-(1-naphthyl)-4-oxobutanoate precursor as a "π-binder" for the porphyrin. The last film was assembled to verify the extendibility of our approach to other *meso*-porphyrins. The proposed structures of the five novel SAMs used in this work are reported in Fig. 3.

UV-Vis spectroscopy

Absorption spectra of SAMs **3–5** on ITO-supported glasses are shown in Fig. 4. These spectra confirmed in all cases the presence of the porphyrin in the monolayer and pointed out significant differences in affinity toward diverse macrocyles and in the binding modality between α and β isomers. Indeed, it is immediately evident from the difference in absorption intensity that tetraphenylporphyrin (H_2TPP) is bound with less affinity than H_2TFcP. This can be ascribed to the absence of an appropriate cavity in H_2TPP able to selectively accommodate

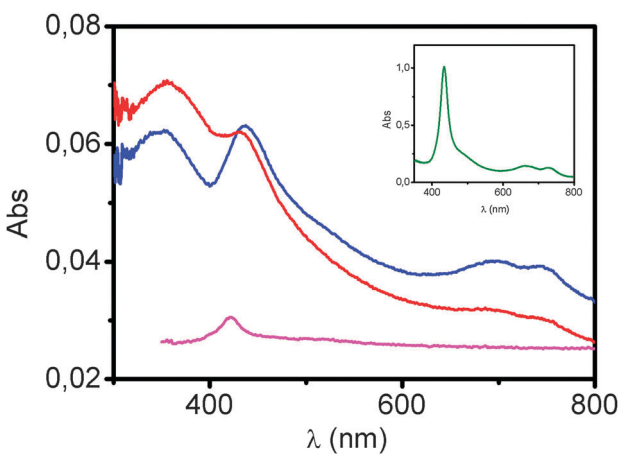

Fig. 4 UV-Vis spectra of SAM **3** (red line), **4** (blue line) and **5** (magenta line). In the inset the absorption spectrum of H_2TFcP in dichloromethane is reported.

the arene rings. Furthermore, the electron density of the *core* of H_2TFcP is lower (as suggested by a much lower shielding effect experienced by inner N–H protons in the ^{1}H NMR spectrum[20]), leading to a lower electrostatic repulsion between π-electron clouds. Also, the strong donor character of H_2TFcP might facilitate a partial charge transfer toward naphthalene. This would lead to a further stabilization of the π-complex. The comparison between the absorption spectra of **4** and **5** reveals that the electronic structure of H_2TPP is less perturbed than that of H_2TFcP upon adsorption on the naphthalene SAM. Indeed, the Soret band of H_2TPP is red-shifted by only 4 nm with respect to its spectrum in dichloromethane (λ_{max} = 417 nm), and its full width at the half of the peak maximum (FWHM) is only slightly increased (22 nm *vs.* 13 nm of the solution value). This accounts for a weak association between the porphyrin and the ligand.

The absorption spectra of **3** and **4** are comparable in intensity and are both dominated by a split and very broad Soret band. This is most likely due to the presence of two different species on surfaces: an aspecifically bound porphyrin, characterised by a Soret band at 437 nm and superimposable to the spectrum in solution; a specifically bound porphyrin, engaged in the formation of a π-complex with the underlying naphthalene monolayer. This latter species is characterised by a largely blue-shifted Soret band centred at about 355 nm. Such a surprisingly intense shift is commonly attributed to face-to-face or H-aggregates of porphyrins[27] and can be tentatively assigned to the formation of a cofacial complex between H_2TFcP and naphthalene. This statement is in accordance with the geometry predicted for the complex by semi-empirical PM3 calculations (see Fig. 1). Also, the width of both the Soret bands reveals an inhomogeneous monolayer in which both the species are likely to give rise to disordered aggregates. It is worth noting that, although the absorption spectra of **3** and **4** are qualitatively identical, the ratio between the Soret bands of the two species is different. Indeed, while the absorption maxima of **4** have basically the same values, the Soret band at 355 nm largely dominates the spectrum of **3**. In other words, the quantity of specifically bound porphyrins in **3** is larger than in **4**. Thus we can conclude that a difference exists in the binding affinity between α and β-naphthalene isomers and, in particular, the arrangement on the surface of the β-substituted "π-binder" is slightly preferred over the disposition assumed by the α isomer. This could be tentatively explained looking at Fig. 1. In fact, in that model of association, the side chain is reasonably expected to have a less steric effect at the β position. Finally, in order to evaluate the specificity of the interaction of the porphyrins with the naphthalene ligands, the absorption spectra of physisorbed H_2TFcP and H_2TPP on ITO were collected. In both cases, the absence of the ligand did not allow the macrocycles to be adsorbed on the oxide surface (see Fig. S10 in ESI‡), thus further confirming the role of naphthalene isomers as specific "π-binders" for *meso*-substituted porphyrins.

Electrochemical properties of films

Cyclic voltammetry (CV) and differential pulse voltammetry (DPV) experiments were carried out in H_2O/Na_2SO_4 using either the modified gold foils or ITO-supported glasses as working electrodes.

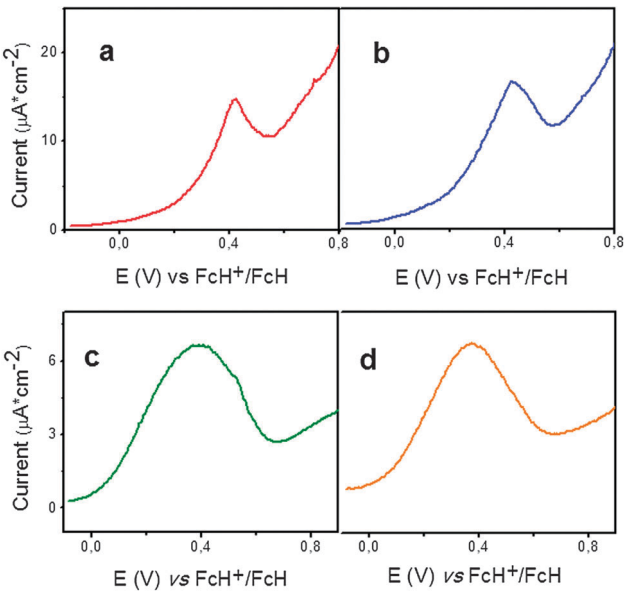

Fig. 5 DPV in H_2O/Na_2SO_4 0.1 M in the oxidative direction of: (a) **1**; (b) **2**; (c) **3** and (d) **4**. Scan rate: 25 mV s^{-1}. Potentials are referred to the couple FcH^+/FcH.

DPVs in the oxidative direction of SAMs **1–4** are shown in Fig. 5. All monolayers showed an intense anodic peak related to the tetraelectronic oxidation of the ferrocenyl groups of H_2TFcP. Indeed, we have previously reported that the oxidation of H_2TFcP is strongly sensitive to the polarity of the medium. In particular, the oxidation potentials of ferrocenes positively shift with the polarity of the solvent.[19] Furthermore, we have shown that the oxidation of chemically equivalent ferrocenyl units in polar media cannot be separated either in solution[19] or on the gold surface.[22] Oxidation of H_2TFcP in SAMs **1–4** occurred at a relatively high potential and a slight positive shift was observed switching from ITO ($E_{1/2}$ = +0.39 V *vs.* FcH^+/FcH) to gold ($E_{1/2}$ = +0.43 V *vs.* FcH^+/FcH). No detectable difference was observed using α or β isomers as ligands for H_2TFcP. Conversely, the shape of the oxidative waves underlines a substantial difference in the homogeneity of the films. As a matter of fact, the full width at the half of the peak maximum (ΔE_{FWHM}) is an important parameter to assess the homogeneity of a monolayer. SAM **1** and **2** gave rise to a sharp oxidation wave ($\Delta E_{FWHM} \approx$ 135 mV), which can be attributed to an ordered monolayer. In fact, in the evaluation of ΔE_{FWHM}, it is necessary to take into account that the width of such a peak is caused by four single-electron oxidations occurring at very close potentials. Also, it should be mentioned that the approach of sulphate counterions to the redox centres, which are buried in a hydrophobic environment, is expected to be partially hampered. This leads to a slow association of the counterions with the porphyrin, thus resulting in the broadening of the peak.[28] In contrast, very broad peaks ($\Delta E_{FWHM} \approx$ 330 mV) were observed using modified ITO electrodes. This reflects a disordered monolayer in agreement with the above-discussed absorption spectra. The broadening of the peak can be explained with the contemporary presence of two species on ITO, being the specifically bound porphyrin in a more hydrophobic microenvironment than the aspecifically adsorbed

Table 1 Densities of porphyrins in SAMs **1–4** measured through the integration of the peaks in DPV experiments

SAM	1	2	3	4
Γ (10^{-10} mol × cm^{-2})	1 ± 0.5	0.8 ± 0.3	0.8 ± 0.3	0.9 ± 0.3

one. Differences in the microenvironment are responsible for the distribution of the formal potentials and, hence, for the widening of the peaks.

The density of macrocycles in the monolayer was attained by the integration of the peaks into DPV experiments. Quite surprisingly, the measured densities (see Table 1) are of the same order of magnitude with respect to that obtained for the same porphyrin covalently attached to the gold surface.[22] Interestingly, no difference in surface coverage of porphyrins was found using α and β isomers as π-binders or on different surfaces. It is worth noting that the values reported above are not referred to specifically bound porphyrins, but to the overall number of molecules on surfaces. Oxidation processes were found to be apparently irreversible in contrast with our previous results on H_2TFcP.[22] Indeed, after the first tetraelectronic oxidation, SAMs become electrochemically silent (see Fig. S11 in ESI‡) and further scans showed no oxidation processes. Instead, the absorption spectra of **3** and **4** were unchanged after DPV and CV experiments (see Fig. S12 and S13 in ESI‡). Such a particular behaviour prompted us to investigate the reasons for the inactivity of electrochemically-generated porphyrin cations. Similarly, Borguet and coworkers observed that the electrochemical activity of oxidised porphyrins was suppressed after physisorption on Au.[29] The electrochemical reversibility was restored holding the potential to a fixed, negative value. The authors explained this peculiar behaviour with a kinetically slow reduction caused by a conformational change that occurred after oxidation. In the light of these results, we decided to repeat a similar experiment. Therefore, after the first DPV experiment with **1**, a negative potential (E = −0.3 V *vs.* SCE) was applied for 30 seconds. At the end of this period a CV experiment was performed and results are shown in Fig. 6. The first scan (red line) exhibited a reversible oxidation process with the reduction occurring around 0 V *vs.* FcH. Such a difference in cathodic and anodic potentials accounts for an electron transfer slower than the scan rate[30] and supports the argument of a slow kinetic of reduction of H_2TFcP when associated with naphthalene. Moreover, the integration of the anodic peak yielded a density of porphyrins of 5.3 × 10^{-11} mol cm^{-2}. Hence, at least half of the macrocycles have restored their electrochemical activity. The intensity of the signals dropped with the number of the experiments and became nil after eight scans (blue line). However, the electrochemical activity was completely reestablished holding the potential to −0.3 V *vs.* SCE for another 30 seconds. Unexpectedly, the same experiment carried out with **3** and **4** did not restore the electrochemical activity of the porphyrins and not even a prolonged exposure (up to 30 minutes) to −0.3 V gave rise to an electrochemical response.

It should be noted that additional peaks appeared in DPV experiments after the application of a negative potential.

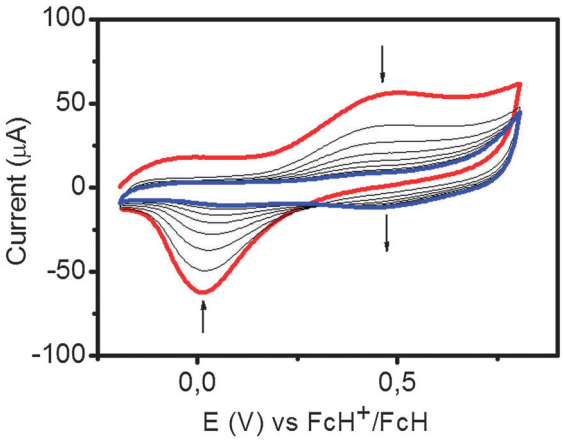

Fig. 6 Subsequent CV scans at 100 mV s^{-1} of **1** in H_2O/Na_2SO_4 0.1 M. The first scan (red line) was carried out after the application of a fixed potential (−0.3 V *vs.* SCE) for 30 s. The last scan is reported in blue. Potentials were adjusted to the couple FcH^+/FcH.

The intensities of the new signals are dependent on the applied potential and on the holding time. To date, the nature of the electrochemically-generated new species is not clear and further investigations on these compounds are currently underway in our laboratories.

Finally, CV and DPV blank experiments were performed after the immersion of the bare gold and ITO electrodes in the porphyrin solution. As expected, physisorption of H_2TFcP occurred on gold[31] and an oxidation was observed in DPV experiments, while no response was detected on ITO (see Fig. S14 and S15 in ESI‡).

X-ray photoelectron spectroscopy (XPS)

XPS spectra in the ionization region of Fe 2p of SAMs **1** (spectra a and b) and **4** (spectra c and d) are reported in Fig. 7. Due to the short inelastic mean free paths of photoemitted electrons upon excitation with soft X-ray sources, XPS is the technique of choice in surface science investigations. In this respect, the thickness of the surface layer explored is very low, in the order of a few nanometers, and depends on the take-off angle (θ). The spectra in Fig. 7 show that the porphyrin derivative is indeed present within the organic monolayers chemisorbed both on Au (spectra a and b) and ITO (spectra c and d). The difference between the couple of spectra a–c and b–d is the value of θ, namely 71° (more surface-sensitive) and 11° (less surface-sensitive), respectively. The Fe 2p XP spectrum can be divided into two regions deriving from the spin–orbit splitting, the J = 3/2 part ranging from ∼705 to ∼718 eV, and the J = 1/2 one between ∼718 and 735 eV BE. Within each of these regions different peaks show up, associated with the same photoemission events. In Fig. 7b, the major contribution comes from the sharp feature at ∼708 eV, associated with Fe(II) centres in the ferrocenyl moieties of H_2TFcP.[24,32] The broader feature centred at ∼711 eV is assigned to Fe(III) of ferrocenium ions in the porphyrin derivative, which is accompanied by its weaker shake-up satellite at around 715 eV. Partial oxidation of ferrocenyl moieties likely occurs upon

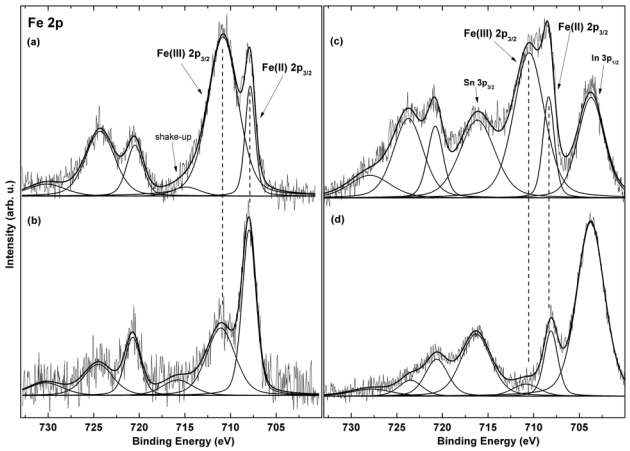

Fig. 7 XP experimental (background corrected) and theoretically reconstructed spectra of Fe 2p region of SAMs **1** (left) and **4** (right). Spectra a and c were acquired at $\theta = 71^\circ$, while spectra b and d at $\theta = 11^\circ$. Vertical dashed lines are drawn to guide the eye in the identification of Fe(II) and Fe(III) components (only in the $J = 3/2$ portion of the spectrum).

exposure to ambient air during sample preparation and was reported several times, especially upon immobilisation reactions on surfaces.[32,33] Upon increase of the θ angle, a more superficial portion of the surface can be investigated. In Fig. 7a, the same photoemission features of the spectrum in Fig. 7b are recorded, but with a sizeable increase of those associated with Fe(III) centres. This dramatic θ-dependency hints at a localization of oxidised ferrocenes at the outer surface of the organic assembly, thus suggesting that oxidation occurred at those Fe sites protruding to the outside environment.

Conversely, the innermost Fe sites, closer to the Au surface, remained protected by the organic SAM. The Fe(II)/Fe(III) atomic ratio, evaluated from peak areas, was 0.98 at $\theta = 11^\circ$ (spectrum b) and 0.22 at $\theta = 71^\circ$ (spectrum a), which suggests that two out of the four ferrocenyl groups are oxidised, provided that the 11° spectrum is taken as indicative of the overall molecule stoichiometry. In fact, the θ-dependency of the Fe 2p signal is itself a proof of the upright standing geometry of the H_2TFcP molecule on the plane of the surface, and, as a consequence, in the spectra at $\theta = 71^\circ$ the Fe(II) photoelectrons are highly attenuated, thus less suitable for a quantitative evaluation. Such a θ-dependency, together with the lack of signals associated with other conformations assumed by the porphyrin, accounts for the formation of a single layer of H_2TFcP interposed between naphthalene units.

In the monolayers assembled onto ITO (spectra c and d), a comparable behaviour can be envisaged with the additional spectroscopical drawback of the features associated with the ITO substrate. In fact, at $\sim$704 and $\sim$717 eV two extra-signals can be found, respectively associated with the ionization of In $3p_{1/2}$ and Sn $3p_{3/2}$ levels from the substrate. The Fe 2p signals do show the same surface enrichment of Fe(III) centres as for the gold surfaces, with a change in the Fe(II)/Fe(III) atomic ratio from 2.8 to 0.26, on going from $\theta = 11^\circ$ (spectrum d) to $\theta = 71^\circ$ (spectrum c). The N 1s and S 2p ionization regions were also recorded for the same samples and their spectra are reported in Fig. S16 and S17 (ESI‡) respectively. Due to the very low intensity of their signals, stemming from very low photoionization cross-sections and high photoelectron attenuation within the organic assembly, their theoretical reconstruction *via* a fitting procedure was not attempted. Nevertheless, their areas served in the calculation of Fe/N and S/Au atomic ratios. The Fe/N ratio, diagnostic of the integrity of the porphyrin derivative both in the gold and ITO samples, gave the following results: 1.4, 0.85 and 1.3, respectively, for the Au samples with α (SAM **2**) and β (SAM **1**) isomers, and for the ITO SAM **4**. Such results, within the associated uncertainty and complications due to photoelectron attenuation, are close to unit and coherent with the theoretical Fe/N ratio. The S/Au ratio for the two gold samples gave the values of 0.076 and 0.077, confirming that the two isomers provide the same coverage on gold.

Further experiments are underway in order to better assess the nature and the origin of the Fe(III) centres within Au and ITO based surface molecular assemblies.

Conclusions

Four novel mixed SAMs were successfully prepared on gold and ITO surfaces exploiting aromatic interactions between *meso*-tetraferrocenylporphyrin and naphthalene. This new approach involves the formation of a naphthalene-containing monolayer to which an unfunctionalised porphyrin is intercalated using a naphthyl scaffold as ''π-binder''. UV-Vis and X-ray photoelectron spectroscopy as well as electrochemical techniques confirmed the specific formation of a π-complex on surfaces. Angle-dependent XPS experiments pointed out the upright geometry assumed by H_2TFcP on the plane of gold and ITO, thus reinforcing the idea of an intercalation among naphthyl units. Not surprisingly, air-exposed ferrocenyl groups were found to be oxidised, whereas SAM-protected moieties retained a Fe(II) centre. Theoretical semi-empirical PM3 geometry optimization showed that naphthalene can be perfectly accommodated into the ''cradle'' formed by the saddle-shaped macrocycle and delimited by two *trans* ferrocenyl groups. In support of this, tetraphenylporphyrin, characterised by a flatter *core*, gave rise to a weaker interaction with naphthalene, as suggested by UV-Vis spectroscopy.

Gold and ITO are not ''innocent'' substrates for the formation of the complex. Indeed, although the density of adsorbed porphyrins is unaltered switching from gold to ITO, a significant difference in terms of homogeneity of the film was observed between the two surfaces. A densely-packed and ordered film was observed on gold, whereas two arrangements of the porphyrins were identified on ITO, namely specifically and aspecifically associated with naphthalene. As a consequence, different electrochemical properties were detected on gold and ITO. The reduction of H_2TFcP engaged in the formation of the complex was found to be kinetically limited on both surfaces. However, the electrochemical activity of the porphyrin can be easily restored through the application of a fixed, negative potential to the modified Au electrodes. Conversely, SAMs on ITO were

found to be electrochemically silent even after a longer exposure to a negative potential.

The encouraging results obtained with this simple approach appear to open a new route for a versatile strategy to deposit other π-conjugated systems onto properly functionalised surfaces.

Experimental

Instruments

UV-Vis data were obtained on a Shimadzu 2450 spectrophotometer. Mass spectra were collected by a GC/MS Shimadzu CP 6000 instrument using a capillary column Supelco SPB-5ms.

NMR spectra were recorded using a Bruker Advance 300 with 300 MHz frequency for protons. Chemical shifts are reported in parts per million and are referred to the residual solvent signal ($CDCl_3$ = 7.28 ppm).

A PalmSense potentiostat was employed in cyclic voltammetry as well as in differential pulse voltammetry experiments.

XPS measurements were performed using a modified Omicron NanoTechnology MXPS system equipped with a monochromatic X-ray anode (Omicron XM-1000), a dual X-ray anode (Omicron DAR 400) and an Omicron EA-127 7-channeltron energy analyser.

Preparation of SAMs

Self-Assembled Monolayers (SAMs) were prepared onto two different surfaces. Glasses with a 100 nm indium tin oxide (ITO) layer were employed in the UV-Vis, XPS and electrochemical characterization, while gold foils (1 × 0.5 cm) were used as the working electrode for electrochemical and XPS experiments. Before the functionalisation, gold foils were immersed for 15 minutes in a "piranha solution" (H_2SO_4–H_2O_2 1 : 1 v/v) while ITO glasses were sonicated for 15 minutes in ethanol. Both the substrates were thoroughly rinsed with distilled water and then with CH_2Cl_2. Gold foils were modified by soaking the electrode in a 1 mM solution of the ligand in CH_2Cl_2 for 20 hours. After this period the surface was thoroughly rinsed with CH_2Cl_2 and immersed in a 1 mM solution of the porphyrin in CH_2Cl_2 for 20 hours. The gold modified electrodes were finally rinsed with CH_2Cl_2 and dried under a nitrogen stream. ITO glasses were functionalised by dipping the surface in a 1 mM solution of the ligand in a THF–MeOH 4 : 1 solution containing 5% NaOH for 20 hours. Such a solution was necessary for an *in situ* hydrolysis of the ester functionality. The surface was then abundantly rinsed with double-distilled water and CH_2Cl_2 and soaked in a 1 mM solution of the porphyrin in CH_2Cl_2 for 20 hours. ITO was finally rinsed with CH_2Cl_2 and dried under a nitrogen stream.

Physical measurements

Absorption spectra were collected using modified ITO glass slides in the range of 300–800 nm. Background subtraction was performed using naphthalene-based SAMs.

Electrochemical measurements were conducted using a three-electrode scheme with SCE as the reference electrode, a platinum wire as the counter electrode and modified gold or ITO surfaces as the working electrodes. A 0.1 M solution of Na_2SO_4 in double-distilled water was chosen as the appropriate solvent–electrolyte couple. Bare gold foils and ITO-supported glasses were employed as the working electrodes in calibration experiments with ferricenium hexafluorophosphate. Potentials were then referred to ferrocene.

The experimental conditions adopted in XPS measurements were: excitation by non-monochromatic Al Kα photons ($h\nu$ = 1486.6 eV) generated at 14 kV, 14 mA, take-off angles (θ) of 11° and 71° with respect to the sample surface normal. The regions associated with ionization of Fe 2p, N 1s, O 1s, C 1s, S 2p, Au 4f levels were acquired using an analyser pass energy of 20 eV, while a survey scan was also taken at 50 eV pass energy. No charging was experienced during measurements. The measurements were performed at room temperature and the base pressure in the analyser chamber was about 2×10^{-9} mbar during the spectral detection. The binding energy (BE) of the C 1s line at 284.8 eV, associated with aromatic carbon, was used as an internal standard reference for the BE scale (accuracy of ±0.1 eV). The experimental spectra were theoretically reconstructed by fitting the secondary electrons background to linear and Shirley functions and the elastic peaks to symmetric Voigt functions described by a common set of parameters (position, FWHM, Gaussian–Lorentzian ratio) let free to vary within narrow limits. XPS atomic ratios between relevant core lines were estimated from experimentally determined area ratios (±10% associated error) corrected for the corresponding Scofield cross sections[34] and for a square root dependence of the photoelectron kinetic energies.

Acknowledgements

The financial support of MIUR PRIN 2010-2011 (no 2010FM738P) is acknowledged. Special thanks to Dr Donato Monti for helpful discussion on UV-Vis spectroscopy of SAMs.

Notes and reference

1 D. M. Crothers and B. H. Zimm, *J. Mol. Biol.*, 1964, **9**, 1; C. A. Hunter, K. R. Lawson, J. Perkins and C. J. Urch, *J. Chem. Soc., Perkin Trans. 2*, 2001, 651.
2 E. Lanzarotti, R. R. Biekofsky, D. A. Estrin, M. A. Marti and A. G. Turjanski, *J. Chem. Inf. Model.*, 2011, **51**, 1623.
3 S. K. Burley and G. A. Petsko, *Science*, 1985, **229**, 23.
4 T. Pullerits and V. Sundström, *Acc. Chem. Res.*, 1996, **29**, 381.
5 T. S. Balaban, H. Tamiaki and A. R. Holzwarth, *Top. Curr. Chem.*, 2005, **258**, 1.
6 Z. Chen, A. Lohr, C. R. Saha-Möller and F. Würthner, *Chem. Soc. Rev.*, 2009, **38**, 564.
7 P. D. W. Boyd and C. A. Reed, *Acc. Chem. Res.*, 2005, **38**, 235; A. L. Litvinov, D. V. Konarev, A. Y. Kovalevsky, I. S. Neretin, P. Coppens and R. N. Lyubovskaya, *Cryst. Growth Des.*, 2005, **5**, 1807; S. Bhattacharya, T. Shimawaki, X. Peng, A. Ashokkumar, S. Aonuma, T. Kimura and N. Komatsu, *Chem. Phys. Lett.*, 2006, **430**, 435; H. Ozawa, X. Yi, T. Fujigaya, Y. Niidome, T. Asano and N. Nakashima, *J. Am. Chem. Soc.*, 2011, **133**, 14771; C. Xue, Y. Xu, Y. Pang,

D. Yu, L. Dai, M. Gao, A. Urbas and Q. Li, *Langmuir*, 2012, **28**, 5956; J.-B. Giguère and J.-F. Morin, *Org. Biomol. Chem.*, 2012, **10**, 1047.

8 J. Song, N. Aratani, H. Shinokubo and A. Osuka, *J. Am. Chem. Soc.*, 2010, **132**, 16356.

9 X. Peng, N. Komatsu, S. Bhattacharya, T. Shimawaki, S. Aonuma, T. Kimura and A. Osuka, *Nat. Nanotechnol.*, 2007, **2**, 361; X. Peng, N. Komatsu, T. Kimura and A. Osuka, *J. Am. Chem. Soc.*, 2007, **129**, 15947; X. Peng, N. Komatsu, T. Kimura and A. Osuka, *ACS Nano*, 2008, **2**, 2045; F. Wang, K. Matsuda, A. F. M. M. Rahman, X. Peng, T. Kimura and N. Komatsu, *J. Am. Chem. Soc.*, 2010, **132**, 10876.

10 T. Hasobe, H. Imahori, P. V. Kamat, T. K. Ahn, S. K. Kim, D. Kim, A. Fujimoto, T. Hirakawa and S. Fukuzumi, *J. Am. Chem. Soc.*, 2005, **127**, 1216; T. Hasobe, P. V. Kamat, V. Troiani, N. Solladie, T. K. Ahn, S. K. Kim, D. Kim, A. Kongkanand, S. Kuwabata and S. Fukuzumi, *J. Phys. Chem. B*, 2005, **109**, 19; H. Imahori, K. Mitamura, Y. Shibano, T. Umeyama, Y. Matano, K. Yoshida, S. Isoda, Y. Araki and O. Ito, *J. Phys. Chem. B*, 2006, **110**, 11399.

11 T. Umeyama, N. Tezuka, F. Kawashima, S. Seki, Y. Matano, Y. Nakao, T. Shishido, M. Nishi, K. Hirao, H. Lehtivuori, N. V. Tkachenko, H. Lemmetyinen and H. Imahori, *Angew. Chem., Int. Ed.*, 2011, **50**, 4615.

12 M. Ohtani, P. V. Kamat and S. Fukuzumi, *J. Mater. Chem.*, 2010, **20**, 582.

13 B. M. J. M. Suijkerbuijk and R. J. M. Klein Gebbink, *Angew. Chem., Int. Ed.*, 2008, **47**, 7396; C. Bucher, C. H. Devillers, J.-C. Moutet, G. Royal and E. Saint-Aman, *Coord. Chem. Rev.*, 2009, **253**, 21; A. Vecchi, P. Galloni, B. Floris and V. N. Nemykin, *J. Porphyrins Phthalocyanines*, 2013, **17**, 165.

14 J. Rochford, A. D. Rooney and M. T. Pryce, *Inorg. Chem.*, 2007, **46**, 7247.

15 C. Bucher, C. H. Devillers, J.-C. Moutet, G. Royal and E. Saint-Aman, *Chem. Commun.*, 2003, 888; C. Bucher, C. H. Devillers, J.-C. Moutet, G. Royal and E. Saint-Aman, *New J. Chem.*, 2004, **28**, 1584.

16 M. Kubo, Y. Mori, M. Otani, M. Murakami, Y. Ishibashi, M. Yasuda, K. Hosomizu, H. Miyasaka, H. Imahori and S. Nakashima, *J. Phys. Chem. A*, 2007, **111**, 5136; V. S. Shetti and M. Ravikanth, *Eur. J. Org. Chem.*, 2010, 494.

17 H. Imahori, H. Norieda, H. Yamada, Y. Nishimura, I. Yamazaki, Y. Sakata and S. Fukuzumi, *J. Am. Chem. Soc.*, 2001, **123**, 100; N. K. Subbaiyan, C. A. Wijesinghe and F. D'Souza, *J. Am. Chem. Soc.*, 2009, **131**, 14646; K. Ikeda, K. Takahashi, T. Masuda and K. Uosaki, *Angew. Chem., Int. Ed.*, 2011, **50**, 1280.

18 D. T. Gryko, F. Zhao, A. A. Yasseri, K. M. Roth, D. F. Bocian, W. G. Kuhr and J. S. Lindsey, *J. Org. Chem.*, 2000, **65**, 7356; J. S. Lindsey and D. F. Bocian, *Acc. Chem. Res.*, 2011, **44**, 638.

19 V. N. Nemykin, G. T. Rohde, C. D. Barrett, R. G. Hadt, C. Bizzarri, P. Galloni, B. Floris, I. Nowik, R. H. Herber, A. G. Marrani, R. Zanoni and N. M. Loim, *J. Am. Chem. Soc.*, 2009, **131**, 14969.

20 V. N. Nemykin, G. T. Rohde, C. D. Barrett, R. G. Hadt, J. R. Sabin, G. Reina, P. Galloni and B. Floris, *Inorg. Chem.*, 2010, **49**, 7497.

21 P. D. W. Boyd, A. K. Burrell, W. M. Campbell, P. A. Cocks, K. C. Gordon, G. B. Jameson, D. L. Officer and Z. Zhao, *Chem. Commun.*, 1999, 637; A. Auger and J. C. Swarts, *Organometallics*, 2007, **26**, 102; G. T. Rhode, J. R. Sabin, D. Barret and V. N. Nemykin, *New J. Chem.*, 2011, **35**, 1440; P. Zhu, X. Zhang, H. Wang, Y. Zhang, Y. Bian and J. Jiang, *Inorg. Chem.*, 2012, **51**, 5651; C. H. Devillers, A. Milet, J.-C. Moutet, J. Pécaut, G. Royal, E. Saint-Aman and C. Bucher, *Dalton Trans.*, 2013, **42**, 1196.

22 A. Vecchi, E. Gatto, B. Floris, V. Conte, M. Venanzi, V. N. Nemykin and P. Galloni, *Chem. Commun.*, 2012, **48**, 5145.

23 G. Baddeley, *J. Chem. Soc.*, 1949, 99.

24 V. N. Nemykin, P. Galloni, B. Floris, C. D. Barrett, R. G. Hadt, R. I. Subbotin, A. G. Marrani, R. Zanoni and N. M. Loim, *Dalton Trans.*, 2008, 4233.

25 J. S. Lindsey, H. C. Hsu and I. C. Schreiman, *Tetrahedron Lett.*, 1986, **27**, 4969.

26 A. L. Eckermann, D. J. Feld, J. A. Shaw and T. J. Meade, *Coord. Chem. Rev.*, 2010, **254**, 1769.

27 J. M. Kroon, R. B. M. Koehorst, M. van Dijk, G. M. Sandersa and E. J. R. Sudhölter, *J. Mater. Chem.*, 1997, **7**, 615; N. C. Mati, S. Mazumdar and N. Periasamy, *J. Phys. Chem. B*, 1998, **102**, 1528; V. Kriegisch and C. Lambert, *Top. Curr. Chem.*, 2005, **258**, 257.

28 J. Jiao, E. Nordlund, J. S. Lindsey and D. F. Bocian, *J. Phys. Chem. C*, 2008, **112**, 6173.

29 T. Ye, Y. He and E. Borguet, *J. Phys. Chem. B*, 2006, **110**, 6141.

30 E. Laviron, *J. Electroanal. Chem.*, 1979, **101**, 19.

31 M. Jurow, A. E. Schuckman, J. D. Batteas and C. M. Drain, *Coord. Chem. Rev.*, 2010, **254**, 2297; J. Otsuki, *Coord. Chem. Rev.*, 2010, **254**, 2311; S. Mohnani and D. Bonifazi, *Coord. Chem. Rev.*, 2010, **254**, 2342.

32 C. M. Woodbridge, D. L. Pugmuir, R. C. Johnson, N. M. Boag and M. A. Langell, *J. Phys. Chem. B*, 2000, **104**, 3085; R. Zanoni, F. Cattaruzza, C. Coluzza, E. A. Dalchiele, F. Decker, G. Di Santo, A. Flamini, L. Funari and A. G. Marrani, *Surf. Sci.*, 2005, **575**, 260; B. Fabre and F. Hauquier, *J. Phys. Chem. B*, 2006, **110**, 6848; F. Decker, F. Cattaruzza, C. Coluzza, A. Flamini, A. G. Marrani, R. Zanoni and E. A. Dalchiele, *J. Phys. Chem. B*, 2006, **110**, 7374.

33 A. G. Marrani, F. Cattaruzza, F. Decker, R. Zanoni, M. Cossi and M. F. Iozzi, *J. Nanosci. Nanotechnol.*, 2010, **10**, 2901; F. Cattaruzza, A. Llanes-Pallas, A. G. Marrani, E. A. Dalchiele, F. Decker, R. Zanoni, M. Prato and D. Bonifazi, *J. Mater. Chem.*, 2008, **18**, 1570.

34 J. H. Scofield, *J. Electron Spectrosc. Relat. Phenom.*, 1976, **8**, 129.

